Buoyant instability of a viscous film over a passive fluid

By D. CANRIGHT[1] AND S. MORRIS[2]

[1] Mathematics, Code MA/Ca, Naval Postgraduate School, Monterey, CA 93943, USA

[2] Mechanical Engineering, University of California, Berkeley, CA 94720, USA

In certain geophysical contexts such as lava lakes and mantle convection, a cold, viscous boundary layer forms over a deep pool. The following model problem investigates the buoyant instability of the layer. Beneath a shear-free horizontal boundary, a thin layer (thickness d_1) of very viscous fluid overlies a deep layer of less dense, much less viscous fluid; inertia and surface tension are negligible. After the initial unstable equilibrium is perturbed, a long-wave analysis describes the growth of the disturbance, including the nonlinear effects of large amplitude. The results show that nonlinear effects greatly enhance growth, so that initial local maxima in the thickness of the viscous film grow to infinite thickness in finite time, with a timescale $8\mu/\Delta\rho g d_1$. In the final catastrophic growth the peak thickness is inversely proportional to the remaining time. (A parallel analysis for fluids with power-law rheology shows similar catastrophic growth.) While the small-slope approximation must fail before this singular time, the failure is only local, and a similarity solution describes how the peaks become downwelling plumes as the viscous film drains away.

1. Introduction

This work examines the strongly nonlinear effects of finite amplitude in the Rayleigh–Taylor instability of a horizontal viscous film under a shear-free boundary and over a much less viscous fluid. Inertia and surface tension are neglected, and, in the parameter range considered, the motion is limited by normal stresses in the more viscous fluid. The analysis exploits the fact that the most unstable wavelengths are long compared to the thickness of the film. The results show how the growth of disturbances to the interface becomes greatly enhanced when the disturbance amplitude becomes large, leading to the formation of downwelling sheets or plumes in a finite time.

The motivation for this problem comes from certain geophysical situations, particularly the stability of the Earth's lithospheric plates. In simplified terms, the oceanic lithosphere (tectonic plates) can be considered a cold, stiff thermal boundary layer above the convecting mantle. Where two plates come together, one subducts under the other and flows downward due to its negative buoyancy. The question of how a new subduction zone is formed, how one large plate may break into two and thus allow some of the dense material to flow back down into the mantle, is not yet resolved. Other closely related geophysical situations include the surfaces of lava lakes, thermal convection in the mantles of other planets, and possibly convection in the Earth's solid core.

This work examines a simple model of one possible mechanism for the initiation of subduction: the Rayleigh–Taylor instability. In this model, the lithosphere and the

mantle are treated as distinct, highly viscous fluids, the lithosphere being denser (and much more viscous) than the mantle. In this unstable configuration, any variations in the lithosphere thickness tend to grow, and when the thickness variations become significant, nonlinear effects cause the growth to accelerate catastrophically, giving downwelling regions (modelling subduction).

A more realistic model of the lithosphere may be a fluid with a power-law rheology, with most of the layer being very stiff, but yielding more readily in regions of rapid deformation. A long-wave analysis for this case (Appendix B) shows that the growth in the deforming regions again becomes catastrophic due to finite-amplitude effects, as in the Newtonian case.

A companion work (Canright & Morris 1993) considers a different model for the lithosphere: as a thermal boundary layer growing under a suddenly cooled horizontal boundary, where the fluid viscosity depends strongly on temperature. The long-wave analysis shows that, again, the nonlinear effects of finite amplitude give catastrophic growth, yielding sheets in finite time. For that case the force balance and the resulting growth of peaks is essentially the same as that considered here, because thermal diffusion becomes unimportant where the layer is thick. The Rayleigh–Taylor problem considered here is the simplest example of this dynamic balance.

The instability of a dense fluid supported by a lighter one has been studied extensively, beginning with the analysis of Rayleigh (1883). Taylor (1950) noted that acceleration would give the same effect as gravity, in agreement with the experiments of Lewis (1950). A thorough introduction to the linear theory is given by Chandrasekhar (1961, chap. X), and recent surveys of previous work are given by Sharp (1984) and Kull (1991). Many of the analyses (e.g. Bellman & Pennington 1954; and Menikoff *et al.* 1978) have focused on the initial small-amplitude growth, where linearized equations are appropriate. One approach for examining the nonlinear effects of large amplitude is direct numerical simulation, e.g. Harlow & Welch (1966) and Tryggvason (1988), or through boundary-integral computations, e.g. Baker & Meiron (1984), and Newhouse & Pozrikidis (1990).

To investigate the nonlinear effects analytically, the most common approach has been the perturbation method, where various quantities are expressed as power series in the small initial amplitude or slope, giving linearized equations for each order (e.g. Emmons, Chang & Watson 1960). However, a wide variety of other methods have been employed (primarily for inviscid fluids) e.g. least-squares approximation (Kull 1986), averaging (Drazin 1969), multiple timescales (Nayfeh 1969), strained coordinates (Amaranath & Rajappa 1976), generalized coordinates (Dienes 1978), Lagrangian formulations (Ott 1972), and heuristic models (Baker & Freeman 1981; Aref & Tryggvason 1989). Also, Dussan V. (1975) used energy methods to determine the stability of disturbances of arbitrary amplitude. In the above studies, inertia is important. The situation we consider, of a thin viscous layer in creeping flow, has been examined primarily in the geophysics literature, e.g. the experiments and weakly nonlinear theory of Whitehead & Luther (1975).

Our analysis is equivalent to a perturbation expansion in the interfacial slope, which for long waves remains small even for large amplitudes. But, unlike the standard approach, the interface position is not expressed as a series; hence the (leading-order) interface conditions are nonlinear, being applied at the moving interface rather than expanded about a plane. In this way the nonlinear effects of finite amplitude are explicitly included. We derive the small-slope equations for three dimensions, and give solutions for the two-dimensional and axisymmetric cases. The results show that thickness maxima grow to infinite thickness in finite time; thereafter the layer drains

through these downwelling regions. (Of course, the small-slope assumption must fail before this, but the failure is localized in asymptotically narrow regions with negligible effects on the dynamics in the rest of the layer.)

2. Problem statement

Two horizontal layers of distinct Newtonian incompressible fluids are bounded above and below by horizontal shear-free boundaries (see figure 1). The upper fluid (of density ρ_1, viscosity μ_1, and average layer thickness d_1) is denser and much more viscous than the lower fluid (of density $\rho_2 < \rho_1$ and viscosity $\mu_2 \ll \mu_1$), and the upper layer is very thin ($d_1 \ll d_2$). Surface tension is neglected, and both fluids are assumed to be so viscous that we can neglect inertia. The former assumption requires that $\gamma k^2 / \Delta\rho g \ll$ 1, while the latter requires $\Delta\rho g L^3 / \rho_2 \nu^2 \ll 1$, where γ is the surface tension, k is the wavenumber, L is the largest lengthscale, $\Delta\rho \equiv \rho_1 - \rho_2$, g is the acceleration due to gravity, and ν is the smaller kinematic viscosity. (The latter restriction is easily satisfied in mantle flow.)

Initially both fluids are at rest in unstable equilibrium. At $t = 0$ the interface is slightly disturbed, after which the position of the interface is $\delta(x, y, t)$. (Long-wave solutions will be given only for the special cases of two-dimensional and axisymmetric disturbances.)

A reduced pressure p is defined in terms of the total pressure P by

$$P(x, y, z, t) = p(x, y, z, t) + \rho_2 g z, \tag{2.1}$$

so that in equilibrium p is a constant in fluid 2. Then the governing equations are

$$\nabla(p + \Delta\rho g z) = \mu_1 \nabla^2 u \quad \text{in fluid 1,} \tag{2.2a}$$

$$\nabla p = \mu_2 \nabla^2 u \qquad \text{in fluid 2,} \tag{2.2b}$$

$$\nabla \cdot u = 0, \tag{2.3}$$

where u is the velocity vector with components (u, v, w). The boundaries exert no shear, and across the interface, which moves as a material surface, both velocity and stress are continuous, hence

$$w = u_z = v_z = 0 \quad \text{at } z = 0 \quad \text{and at} \quad z = d_1 + d_2, \tag{2.4a}$$

$$[u]|_1^2 = 0 \qquad \text{at } z = \delta(x, y, t), \tag{2.4b}$$

$$[\sigma_{ij} n_j]|_1^2 = 0, \tag{2.4c}$$

$$\delta_t + u\delta_x + v\delta_y = w, \tag{2.4d}$$

where subscripts indicate partial derivatives, the brackets $[\,]|_1^2$ indicate the change in the enclosed quantity across the interface from fluid 1 to fluid 2, σ_{ij} is the reduced stress tensor (using the reduced pressure p), and n is a unit vector normal to the interface, with components n_i. (If the upper boundary is instead a free surface with no shear and zero pressure, then in the long-wave analysis below, the surface deflection is proportional to the two-fluid interface deflection in the ratio $\Delta\rho/\rho$, which is assumed to be small. Also note that the boundary condition at $z = d_1 + d_2$ is irrelevant to the long-wave analysis below, provided fluid 2 is sufficiently deep.) Specification of the initial interface position $\delta(x, y, 0)$ completes the problem definition.
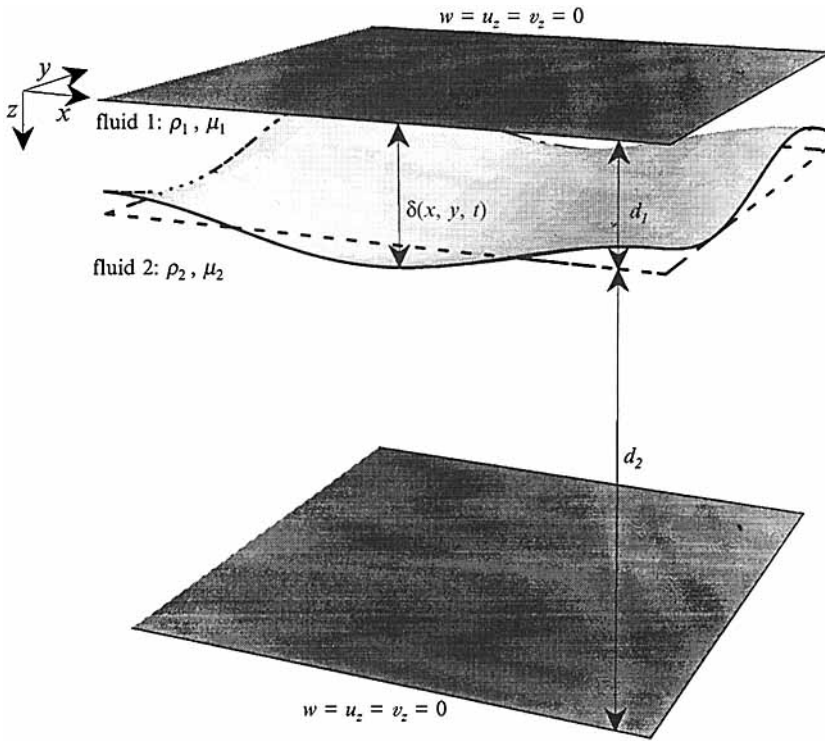
FIGURE 1. Problem description. Between two horizontal, shear-free planes, a layer of fluid 1 of uniform thickness d_1 is initially in unstable equilibrium over a layer of fluid 2 of thickness d_2. The upper layer is denser ($\rho_1 > \rho_2$), much thinner ($d_1 \ll d_2$), and much more viscous ($\mu_1 \gg \mu_2$). After the interface is perturbed, its position is given by $\delta(x, y, t)$.

3. Long-wave analysis

The disturbance can grow in a variety of ways, depending on the viscosity ratio, the depth ratio, and the dimensionless wavenumber:

$$\alpha \equiv \mu_2/\mu_1, \quad \beta \equiv d_2/d_1, \quad \epsilon \equiv kd_1 \tag{3.1}$$

where the disturbance has a characteristic wavenumber k. Here we focus on the case where the lower fluid layer is much less viscous and deeper than the upper ($\alpha \ll 1$, $\beta \gg 1$).

The linearized small-amplitude solution given in Appendix A shows that for this case the fastest growing wavelength is long compared to d_1. In fact, the linearized growth rate is nearly constant over a broad range of wavelengths:

$$\max{(\alpha, (\alpha/\beta)^{\frac{1}{2}})} \ll \epsilon \ll 1 \tag{3.2}$$

as illustrated in figure 7(a). In this range, the growth is limited by normal stresses in the upper fluid, which moves nearly horizontally, while the lower fluid is passively moved by the interface. Outside this range, for waves short compared to d_1, the growth is reduced because only a fraction of layer 1 is mobilized, and for long enough waves the viscous resistance of fluid 2 slows the growth.

We examine the finite-amplitude growth of long-wave disturbances in this fastest-growing range, exploiting the fact the slope of the interface remains small even for large amplitudes (until the disturbance grows to the order of the initial wavelength). What follows is the leading-order asymptotic analysis, containing only the dominant balance

of forces. This balance is insensitive to wavelength (the linearized growth rate is constant to within $O(\epsilon^4)$), so this analysis cannot predict the single wavelength giving maximum growth.

The small slope of the interface greatly simplifies the dynamics of the thin upper layer, which controls the growth. In fluid 1, the horizontal lengthscale (k^{-1}) is much larger than the vertical (d_1), so by continuity the horizontal velocity components (scale U, say) are large relative to the vertical components (ϵU). The momentum equation implies that the vertical variation of reduced pressure is negligible ($O(\epsilon)$) compared to horizontal variations.

In fluid 2, the horizontal velocity and length scales are those of the interface (U and k^{-1}); the vertical lengthscale is comparable (except for waves long compared to d_2, where the depth is the vertical scale). Then the shear stress from fluid 2 scales as $\mu_2 u_z \sim \mu_2 kU$ (or $\sim \mu_2 U/d_2$ in the latter case). Since the shear in fluid 1 scales as $\mu_1 u_z \sim \mu_1 w_x \sim \mu_1 \epsilon kU$, then the shear from fluid 2 will be negligible provided $\alpha \ll \epsilon$ (or $\alpha/\beta \ll \epsilon^2$ if $\beta\epsilon < 1$), which is just the lower bound on wavenumber assumed above. For wavelengths in this range, the interface motion is controlled by the dynamics of the upper fluid, for which the lower fluid is effectively passive and hydrostatic.

Then in layer 1, both the upper boundary and the interface appear shear-free, so the horizontal velocity components are independent of z (to $O(\epsilon^2)$), as are the components $\tau_{xx}, \tau_{xy}, \tau_{yy}, \tau_{zz}$ of the deviatoric stress tensor τ_{ij}. (This scaling analysis is extended to other wavelengths in Canright 1987.)

While the long-wave equations can be derived by expanding the velocity and stress in powers of ϵ, the meaning of the result is better understood as a force balance on a small column of layer 1, as shown in figure 2. Here only horizontal forces are considered, and as before the total stress everywhere has been reduced by the hydrostatic pressure of fluid 2, which does not affect the horizontal balance. Then there are no forces acting on the top and bottom of the column, and so the net force acting on the sides must be zero. The differential form of this balance can be written in terms of a two-dimensional reduced force tensor F_{ij} which results from integrating the reduced stress tensor across the layer

$$F_{ij} \equiv \int_0^\delta [-(p+\Delta\rho gz)\,\delta_{ij}+\tau_{ij}]\mathrm{d}z, \quad i,j = 1,2, \tag{3.3}$$

where δ_{ij} is the Kronecker delta. The normal stress condition at the interface,

$$-(p+\Delta\rho g\delta)+\tau_{zz} = 0 \quad \text{at} \quad z = \delta \tag{3.4}$$

can be used to eliminate p, so the reduced force is

$$F_{ij} = \delta(-\bar{P}\delta_{ij}+\tau_{ij}), \tag{3.5a}$$

$$\bar{P} \equiv -\tfrac{1}{2}\Delta\rho g\delta+\tau_{zz}, \tag{3.5b}$$

where $\bar{P}$ is the average pressure and τ_{zz} is evaluated at the interface. Then the horizontal force balance means the reduced force tensor has zero divergence:

$$F_{ij,j} = 0, \quad i,j = 1,2. \tag{3.6}$$

The kinematic interface condition becomes, on eliminating w using continuity,

$$\delta_t + (\delta u)_x + (\delta v)_y = 0. \tag{3.7}$$

These two equations (along with conditions at the edges of the layer) govern the growth of long-wave disturbances, including the nonlinear effects of finite amplitude, with a
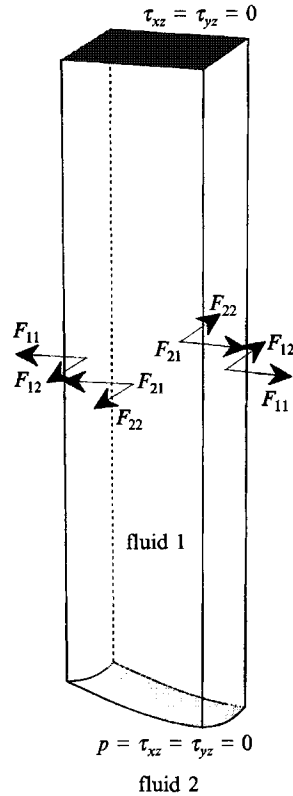
FIGURE 2. Balance of horizontal forces, reduced by the hydrostatic pressure gradient of fluid 2, on a differential column of fluid 1. Because there is no shear above or below and no (reduced) pressure below, the reduced horizontal force tensor F_{ij} acting on the vertical surfaces of the column has zero divergence.

relative error of $O(\epsilon)$. This conclusion is independent of rheology, and relies only on the small-slope approximation (valid until amplitudes are comparable with the wavelength) and the assumption that fluid 2 is dynamically unimportant.

The dimensionless form of (3.6) becomes, for Newtonian rheology,

$$[\delta^2 + \delta(u_x + \tfrac{1}{2}v_y)]_x + \tfrac{1}{4}[\delta(u_y + v_x)]_y = 0, \tag{3.8a}$$

$$[\delta^2 + \delta(v_y + \tfrac{1}{2}u_x)]_y + \tfrac{1}{4}[\delta(u_y + v_x)]_x = 0, \tag{3.8b}$$

while (3.7) remains the same under non-dimensionalization. (A fluid with power-law rheology is considered in Appendix B.) Here we used a vertical lengthscale of d_1, a timescale of $8\mu/\Delta\rho g d_1$ (corresponding to half the small-amplitude growth rate), and any horizontal lengthscale. In this simplified problem, the layer thickness δ is analogous to variable density, as shown by (3.7), but also acts somewhat like variable viscosity, as well as a body force, in (3.8).

If the initial disturbance to the interface is axisymmetric or varies only in one direction, the dimensionality of the problem is further reduced, allowing simpler solutions to illustrate the nonlinear dynamics. The axisymmetric equations are

$$[\delta^2 + \delta(ru)_r/r]_r = \tfrac{1}{2}\delta_r \frac{u}{r}, \tag{3.9}$$

$$\delta_t + (r\delta u)_r/r = 0, \tag{3.10}$$

where u is the radial velocity component and r the radial coordinate.

The long-wave versions of the two-dimensional equations

$$(\delta^2 + \delta u_x)_x = 0,$$ (3.11)

$$\delta_t + (\delta u)_x = 0,$$ (3.12)

allow greater simplification. The first shows that the reduced force (scalar) $F \equiv \delta^2 + \delta u_x$ acting on any vertical cross-section of the layer is independent of position, though it may depend on time; the value of $F(t)$ depends on the conditions at the ends of the layer.

We can eliminate u by adopting a Lagrangian formulation, where the fluid 'particle' in this case is a material cross-section of the layer. Then the new variables are (x_0, t), where x_0 refers to a particular fluid section by its initial position. The resulting ordinary differential equation describes the growth of a moving cross-section:

$$D\delta/Dt = \delta^2 - d_e^2(t),$$ (3.13)

where $D\delta/Dt \equiv \delta_t + u\delta_x$ and $d_e(t) \equiv (F(t))^{\frac{1}{2}}$ is the current equilibrium thickness, i.e. that with no tendency to grow or shrink. This result shows that the vertical motion of the interface depends only on the local layer thickness and the current equilibrium thickness (which may depend on the overall shape of the whole layer). Thus any fluid cross-section does not care what its immediate neighbours are doing, and the growth is insensitive to wavelength, as expected.

The horizontal motion of a cross-section depends on the state of the whole layer. The position of each fluid cross-section can be followed by integrating the strain. By conservation of mass, $\delta_0 \, dx_0 = \delta \, dx$, where $\delta_0(x_0) = \delta(x_0, t = 0)$ is the initial thickness of the section, so the strain is $dx/dx_0 = \delta_0/\delta$ and the position is given by

$$x(x_0, t) = \int_0^{x_0} \frac{\delta_0(\xi_0)}{\delta(\xi_0, t)} \, d\xi_0,$$ (3.14)

where the x origin is chosen at some stationary fluid cross-section.

4. Solutions

To show most clearly the effects of finite amplitude, we concentrate on the simplest situation, where the initial disturbance depends only on x. We give solutions to (3.13) for three types of conditions at the ends of the layer, for which $d_e(t)$ is simple to evaluate. For the first, the layer is of infinite extent but the disturbance is localized, so that far away the layer remains in (unstable) equilibrium, and $d_e = 1$. Next is the case of a periodic disturbance; then $d_e(t)$ is an integral property of the shape of the layer. The third case treats a layer of finite extent, with abrupt ends surrounded by fluid 2, so $d_e = 0$; this solution also applies approximately whenever δ grows large enough that d_e is negligible. Lastly, to illustrate one significant difference when the disturbance varies in more than one direction, we show a solution to (3.9), (3.10), the axisymmetric case.

4.1. *Localized disturbance*

The most illustrative case is an infinite layer with a disturbance of finite extent. Then the force on the ends of the disturbed region remains constant: $d_e = 1$. This gives a simple solution:

$$\delta(x_0, t) = \frac{\delta_0(x_0) - \tanh(t)}{1 - \delta_0(x_0) \tanh(t)},$$ (4.1)

where again δ_0 is the initial thickness and x_0 the initial position of a fluid section. This solution predicts a singularity in finite time: at the critical time $t_* \equiv \frac{1}{2}\ln|(\delta_0+1)/(\delta_0-1)|$ the thickness δ goes to ∞ or 0, depending on whether the initial thickness δ_0 was greater or less than 1. (Of course, the small-slope approximation must fail when the peak thickness gets large enough; this point is addressed in the next section.)

The early growth of a disturbance of small amplitude $a(x_0, t) \equiv \delta(x_0, t) - 1$ is roughly

$$a(x_0, t) \approx a_0(x_0)\,e^{2t}[1 + \tfrac{1}{2}a_0(x_0)\,(e^{2t}-1)].\tag{4.2}$$

Initially this gives the exponential growth of the linearized solution, but as nonlinearities become important the perturbation growth accelerates for peaks $(a > 0)$ and retards for troughs $(a < 0)$. To preserve volume, the peaks get narrower and sharper while the troughs broaden and flatten. A rough estimate for the duration of the linear behaviour is $\Delta t \sim \frac{1}{2}\ln|1/a_0|$.

As the amplitude gets large, the growth becomes algebraic in the time remaining before the singularity at time t_*:

$$\delta \approx 1/(t_*-t), \quad \delta_0 > 1,\tag{4.3a}$$

$$\delta \approx t_*-t, \quad \delta_0 < 1,\tag{4.3b}$$

which shows that the rapid nonlinear growth occurs over a timescale $\Delta t \sim 1$, or, dimensionally, $8\mu/\Delta\rho g d_1$.

The catastrophic growth shown by the inverse relation (4.3a) between peak thickness and remaining time is strikingly different from the exponential growth of small amplitudes. For large peaks the relevant timescale is inversely proportional to the current peak thickness; thus large-amplitude effects drastically enhance the growth of peaks.

Another effect of finite amplitude is that the overall strain increases, i.e. the disturbed section stretches in the x-direction. In fact, it can be shown (using the Schwarz inequality), that for any initial perturbation with a zero mean, the length of the perturbed section increases continually. This surprising behaviour does not apply in general, but rather is a direct consequence of the assumption that the force on the ends remains constant.

As an example, if the initial perturbation is sinusoidal then

$$\delta_0 = 1 + b\cos x_0,\tag{4.4a}$$

$$\delta(x_0, t) = \frac{2 + b(1 + e^{2t})\cos x_0}{2 + b(1 - e^{2t})\cos x_0},\tag{4.4b}$$

$$x(x_0, t) = -b\tanh(t)\sin(x_0) + (\mathrm{sech}^2(t) - \tanh(t))\,x_0$$

$$+ \frac{2\tanh(t)\,\mathrm{sech}(t)}{[e^{-2t} - b^2\cosh^2(t)]^{\frac{1}{2}}}\arctan\left(\left[\frac{e^{-t} - b\cosh(t)}{e^{-t} + b\cosh(t)}\right]^{\frac{1}{2}}\tan\left(\tfrac{1}{2}x_0\right)\right)\tag{4.4c}$$

and the overall strain is $\mathrm{sech}^2(t) - \tanh(t) + 2\tanh(t)\,\mathrm{sech}(t)/[e^{-2t} - b^2\cosh^2(t)]^{\frac{1}{2}}$, which increases monotonically with time. The layer shapes for one wavelength of this solution at various times are shown in figure 3; as the growth becomes nonlinear the wavelength stretches out. If the initial amplitude b is small, the solution simplifies:

$$\delta \approx \frac{1 + \frac{1}{2}b\,e^{2t}\cos x_0}{1 - \frac{1}{2}b\,e^{2t}\cos x_0},\tag{4.5a}$$

$$x \approx \frac{4}{[1 - (\frac{1}{2}b\,e^{2t})^2]^{\frac{1}{2}}}\arctan\left(\left[\frac{1 - \frac{1}{2}b\,e^{2t}}{1 + \frac{1}{2}b\,e^{2t}}\right]^{\frac{1}{2}}\tan\left(\tfrac{1}{2}x_0\right)\right) - x_0.\tag{4.5b}$$
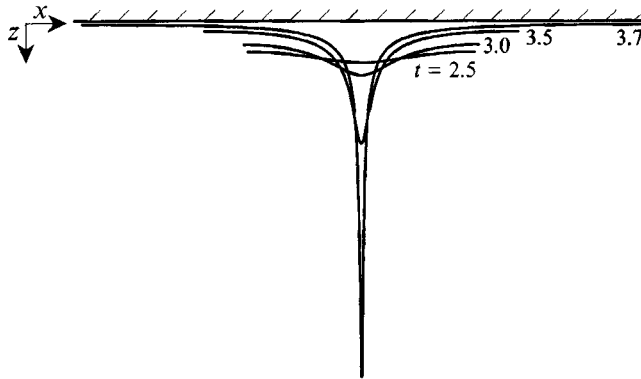
FIGURE 3. Interface profiles $\delta(x)$ at various times ($t = 2.5, 3.0, 3.5, 3.7$) following the evolution of one wavelength of an initial sinusoidal perturbation of amplitude 10^{-3}, for the constant-end-force condition ($F = 1$). (Here the peak reaches infinite thickness at $t_* = 3.80$.) As nonlinear effects become important, the peak sharpens while the troughs flatten and widen; also the wavelength increases over time.

4.2. Constant-wavelength disturbance

For the second case, we enforce the more physically reasonable condition that the wavelength of the disturbance remain constant over time. (This could apply either to a periodic disturbance of infinite extent, or to a layer of finite extent bounded by fixed shear-free endwalls.) Then the reduced force in the layer must vary with time to give zero velocity at both ends of one wavelength. Integrating (3.11) in x shows that fixed ends require

$$d_e^2(t) = \int_0^L \delta \, dx \bigg/ \int_0^L 1/\delta \, dx, \qquad (4.6)$$

where L is one wavelength, and the numerator is just the total volume of fluid in the layer over that wavelength, and so remains constant. Thus the thinnest parts of the layer have the greatest effect on the current equilibrium thickness $d_e(t)$. We find that the constant wavelength requirement causes the equilibrium thickness $d_e(t)$ to decrease in over time (the proof again involves the Schwarz inequality).

Eliminating d_e from (3.13) (and using $\delta \, dx = \delta_0 \, dx_0$) gives a single partial integro-differential equation:

$$\frac{D\delta}{Dt} = \delta^2 - \int_0^L \delta_0 \, dx_0 \bigg/ \int_0^L \delta_0/\delta^2 \, dx_0. \qquad (4.7)$$

Again, the local growth depends only on the relation between the local thickness and an integral property of the entire disturbance, but is independent of the immediate neighbourhood.

For large amplitude, the main effect of fixed wavelength is to slow the growth of troughs; in fact, the thickness δ is prevented from reaching zero. In contrast, peak growth is only slightly accelerated. When peaks become large, then the equilibrium thickness d_e becomes negligible in comparison, as in the constant-d_e case, but sooner here since d_e decreases. Thus large peaks show the same catastrophic growth to infinite thickness, given by (4.3a). The growth of large peaks, where d_e is unimportant, is insensitive to end conditions, and our previous conclusion, that the growth of peaks is dramatically enhanced by large-amplitude effects, applies in general.
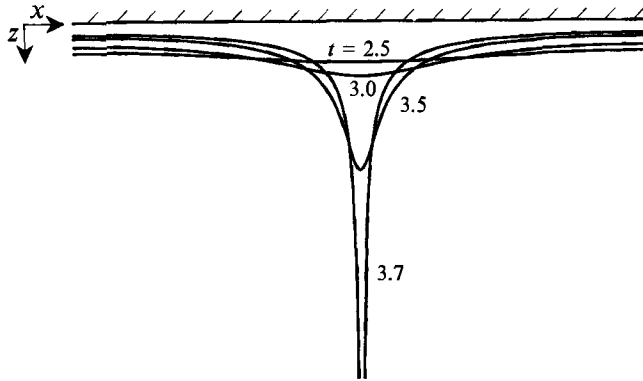
FIGURE 4. Interface profiles for the constant-wavelength end condition ($L = 1$). Similar to figure 3, except that the troughs become thin more slowly, the peaks reach infinite thickness slightly sooner (at $t_* = 3.74$), and the wavelength remains constant.
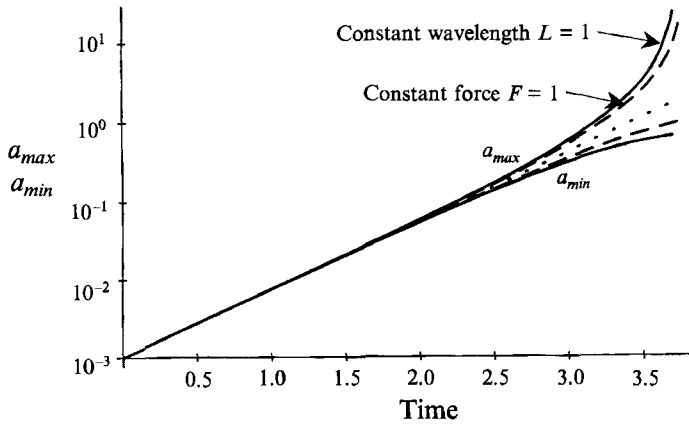

FIGURE 5. Growth of the disturbance amplitude over time for an initial perturbation amplitude of 10^{-3}. Both the peak amplitude $a_{max} = \delta_{max} - 1$ and the trough amplitude $a_{min} = 1 - \delta_{min}$ are shown: constant-wavelength condition (solid), constant end-force (dashed), and linearized (exponential) growth (dotted), for comparison. The constant-wavelength condition tends to destabilize peaks but stabilize troughs relative to the constant-force condition.

Qualitatively this case is very similar to the previous, as shown by the profiles in figure 4, except that the wavelength remains constant. Figure 5 compares the growth of the disturbance for fixed wavelength with that for constant end forces, each for an initial small sinusoidal disturbance.

4.3. Large-amplitude behaviour

Where $\delta \gg d_e$, we can approximate (3.13) by

$$D\delta/Dt = \delta^2. \tag{4.8}$$

(This would also apply if the layer were of finite extent, surrounded by fluid 2, so $d_e = 0$.) The solution

$$\delta(x_0, t) = \frac{1}{[1/\delta_0(x_0)] - t} \tag{4.9}$$

shows each cross-section reaching infinite thickness in a finite time $t = 1/\delta_0$; this is the same growth as (4.3*a*).

For this case, (3.11) integrates to

$$u(x, t) = -\int_0^x \delta(\xi, t)\,\mathrm{d}\xi \tag{4.10}$$

and as long as δ remains finite everywhere, we can express this in Lagrangian coordinates as

$$u(x_0, t) = -\int_0^{x_0} \delta_0(\xi_0)\,\mathrm{d}\xi_0. \tag{4.11}$$

Hence each cross-section moves at a uniform speed over time. These results apply locally around any large peak where d_e is negligible.

4.4. *Axisymmetric growth*

How does the three-dimensional case differ from the two-dimensional solutions above? One difference is that the reduced force is a tensor that varies with position, rather than a uniform scalar. Consequently, two separate portions of the layer having the same thickness may not grow at the same rate. Another difference is the possibility of (vertical) vorticity and shear stresses in the layer.

Here, we examine the growth of an axisymmetric disturbance without swirl. Then the reduced force tensor F_{ij} is diagonal in the (r, θ)-coordinates, without shear, and has radial and circumferential components

$$F_{11} = \delta^2 + \delta(u_r + \tfrac{1}{2}u/r), \tag{4.12a}$$

$$F_{22} = \delta^2 + \delta(\tfrac{1}{2}u_r + u/r), \tag{4.12b}$$

where u is the radial velocity. The radial force balance (3.9) can be expressed as

$$(F_{11})_r + \tfrac{1}{2}\delta(u/r)_r = 0. \tag{4.13}$$

The axisymmetric equations (3.9), (3.10) apparently have no simple closed-form solutions, except when the layer is of uniform thickness. In this special case, $u \propto r$, so F_{11} is uniform, and the thickness grows according to

$$\mathrm{d}\delta/\mathrm{d}t = \tfrac{4}{3}(\delta^2 - F_{11}(t)). \tag{4.14}$$

Comparing with (3.13) shows that the axisymmetric growth of a flat layer is qualitatively identical to (though one-third faster than) the two-dimensional case for comparable force conditions on the boundary. This special case may be indicative of the dynamics of a smooth peak at the origin; in numerical solutions the growth of large peaks approaches the inverse time behaviour $\delta \propto 1/(t_* - t)$, where the constant of proportionality is of order unity.

We have solved the axisymmetric equations numerically for two different edge conditions and a variety of initial conditions. For a localized disturbance, at the edge of the disturbed disk $(ru)_r = 0$ to balance the force in the surrounding undisturbed layer. As in the two-dimensional version, the disturbed region tends to spread out since the broadening of the troughs overwhelms the narrowing of the peaks. For a disturbance of fixed radial extent, then at the edge $u = 0$; this case is a circular approximation of one hexagonal cell of a periodic array, such as seen in the experiments of Whitehead & Luther (1975). Again, the spatial constraint limits the deepening of troughs, while slightly accelerating the growth of peaks. In figure 6, we
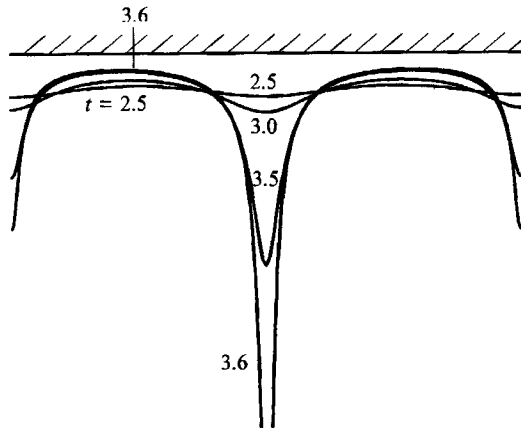
FIGURE 6. Interface profiles $\delta(r)$ for an initial axisymmetric sinusoidal perturbation of amplitude 10^{-3}, where the disturbance is contained within a constant radius ($R = 1$). The central peak grows more quickly than the outer ring-shaped peak of the same initial amplitude.

show profiles for this case, started from a radial sinusoid. This shows that the central peak grows faster than the ring-shaped outer peak, though they begin with identical amplitudes.

For all of the axisymmetric cases we have calculated, the qualitative behaviour is similar to the two-dimensional versions, in that the nonlinearity leads to broad, flat troughs between sharpening peaks whose growth accelerates to an inverse-time catastrophe. One difference, however, is that the growth is no longer merely a function of local thickness, but also depends on position. For the general three-dimensional case, we would expect nonlinear growth to yield broad depressions separating sharp peaks and ridges growing catastrophically into plumes and sheets, although there could be additional effects due to shear and swirl.

5. Vertical sheet formation

Here we examine what happens in the two-dimensional case when a thickness maximum approaches infinite thickness at the singular time t^*. We will show how the peak becomes a vertical sheet, where the dense viscous fluid drains down. The small-slope equations still describe the behaviour in most of the layer, except in an asymptotically narrow neighbourhood of the sheet, because the sheet has only an asymptotically small effect on the stress in the layer.

As a peak grows, the small-slope assumption must break down locally before the peak reaches infinite thickness. Since the initial disturbance wavelength is long compared to the layer thickness, then when the peak grows larger than a wavelength, that portion of the layer around the peak where the physical slope of the interface is $O(1)$ or greater must be asymptotically narrow compared to the whole wavelength. This follows from mass conservation, and from the shape near the peak approaching (as we will show) an integrable negative power of x (where $x = 0$ at the peak). Therefore the small-slope approximation continues to apply almost everywhere in the layer; what is needed is a description of the effect of the peak or sheet on the rest of the layer.

In an earlier work (Canright 1987) we give a large-slope analysis appropriate to the region around a peak where the small-slope approximation no longer applies. (The approach used there is essentially that of Wilson 1988.) Assuming that the interface is

nearly vertical, then the flow is extensional, driven by negative buoyancy and limited by normal viscous stresses. We find that large-slope effects do not slow down the growth, they only affect the details of the peak shape. Indeed, the catastrophic growth described by (4.3 a) still applies (except for a numerical coefficient of $O(1)$ depending on the shape). Physically, there is nothing to prevent the fluid from flowing down, and so the peak extends to become a sheet. Of course, at some point the extending peak either will reach the lower boundary or will become so long that the viscous resistance of fluid 2 becomes important. In the former case, a pool forms, without any effect on the upper layer, but in the latter, the flow driven in fluid 2 could alter the dynamics of the upper layer.

To the rest of the layer the sheet appears as an isolated singularity, a sink of fluid. The horizontal force balance must still apply even to the sheet, and so the reduced force in the layer $F(t)$ is continuous across the sheet. In general $F(t)$ is an integral property of the whole layer, for example (4.6) for a fixed-wavelength disturbance, where the troughs have a greater influence than the peaks. Because the large-slope region is integrable (as it must be, since no new mass is created) and asymptotically thin, its effect on $F(t)$ is negligible.

As an example of the formation of a peak singularity, consider what happens when the initial disturbance is a small-amplitude sinusoid. (From simplicity, we assume the constant-force end conditions, but since F has little effect on a large peak the results apply to more general end conditions.) The previous solution (4.5) shows that the peak becomes singular as $\frac{1}{2}b\,e^{2t}$ approaches unity. In that limit, (4.5 a, b) become

$$\delta \approx \cot^2(\tfrac{1}{2}x_0), \qquad x \approx 2\tan(\tfrac{1}{2}x_0) - x_0. \qquad (5.1\,a, b)$$

Then near the peak ($x_0 \ll 1$)

$$x \approx \tfrac{1}{12}x_0^3 \qquad (5.1\,c)$$

and so

$$\delta \approx (\tfrac{1}{2}x_0)^{-2} \approx (3/2x)^{-\frac{2}{3}}. \qquad (5.1\,d)$$

This shows that at the singular time the peak becomes proportional to an integrable negative power of x, specifically $\delta \propto x^{-\frac{2}{3}}$.

In fact, the same power of x results from any smooth initial peak that locally can be fit by a parabola. As the singular time is approached, the peak can be described by a similarity solution, as shown in Appendix C. The general similarity solution shows that a peak of the more general form $\delta_0 \approx 1 + b(1 - c|x_0|^n)$, where $n > 0$, gives a singularity of the form $\delta(x, t_*) \propto |x|^{-m}$, where $m \equiv n/(n+1)$. Hence any initial peak becomes, at t_*, a singularity proportional to an integrable negative power of x.

To follow how fluid flows into the sheet, the large-amplitude equations (4.9), (4.10) apply near the sheet (but outside the large-slope region). After t_*, there is a singularity (the sheet) at the origin, and the layer must move in such a way that each fluid cross-section reaches the singularity at the same time that it reaches infinite thickness. This determines the strength of the mass sink over time.

Consider the fate of the inverse power of x singularity that forms at t_*. This is most simply described if we take the state of the layer at t_* to be the new reference state, and relabel each fluid cross-section x_0 by its new reference position $x_* \equiv x(x_0, t_*)$, with reference thickness $\delta_*(x_*) \equiv \delta(x, t_*)$, so

$$\delta_*(x_*) \equiv \delta(x = x_*, t = t_*) = bx_*^{-m}, \quad 0 < m < 1 \quad \text{at} \quad \tau = 0 \qquad (5.2a)$$

where $\tau \equiv t - t_*$ and b is some positive amplitude. Then the fluid cross-section that arrives at the singularity at time τ is that which becomes infinitely thick at that time; we call this section $x_s(\tau)$: $x(x_* = x_s(\tau), \tau) = 0$. Using (4.9) gives

$$x_s(\tau) = (b\tau)^{1/m}, \qquad \delta(x_*, \tau) = b/(x_*^m - x_s^m) \qquad (5.2b, c)$$

and so

$$x(x_*, \tau) = \int_{x_s}^{x_*} \frac{\delta_*(\xi_*)}{\delta(\xi_*, \tau)} d\xi_* = (x_* - x_s) - \frac{x_s^m}{1-m}(x_*^{1-m} - x_s^{1-m}). \qquad (5.2d)$$

Away from the sheet ($x_* \gg x_s$), the profile is still the starting profile from $\tau = 0$ ($x \approx x_*$, $\delta \approx bx^{-m}$). However, very close to the sheet

$$x \approx \tfrac{1}{2}mx_s\epsilon^2 \qquad \qquad \Big\} \qquad \text{for} \quad \epsilon \equiv (x_*/x_s - 1) \ll 1. \qquad \begin{matrix} (5.2e) \\ (5.2f) \end{matrix}$$
$$\delta/b \approx 1/(mex_s^m) \approx (b\tau)^{\frac{1}{2}m-1}/(2mx)^{\frac{1}{2}} \Big\}$$

This shows that very near the sheet, the singularity goes like $1/x^{\frac{1}{2}}$, with a scale that varies in time. (This local x-dependence is actually independent of the starting conditions, as shown in Canright 1987, Appendix C.) From (5.2f) it is clear that whether the thickness around the sheet grows or shrinks is determined by whether $m < \frac{1}{2}$ or $m > \frac{1}{2}$, respectively.

The special case $m = \frac{1}{2}$ gives a steady solution. For $m > \frac{1}{2}$, the fluid drains away down the sheet faster than it comes in from the sides, and the square-root singularity diminishes with time as it spreads out, to match onto the nearly undisturbed profile x^{-m}. This would be the eventual fate of an initially ($t = 0$) smooth maximum, which gives $m = \frac{2}{3}$. Conversely, if $m < \frac{1}{2}$, the square-root singularity grows as it spreads, fed from the sides faster than it can drain fluid away. (To get $m < \frac{1}{2}$ would require a cusp-like initial [$t = 0$] maximum, which may not be physically realistic.) This solution (5.2) is again a particular case of the general large-amplitude similarity solution of Appendix C.

(For the axisymmetric case, there is no similarity solution that describes how a finite peak grows into a plume, but we speculate that the same qualitative behaviour applies. A steady axisymmetric plume has the shape $\delta \propto 1/r$.)

With the above description of how a sheet first forms and how it behaves afterward, the small-slope equations can be used to follow the development of the instability from initial conditions through rapid large-amplitude growth all the way to the draining away of the fluid down the sheets. The results will be inaccurate wherever the physical slope of the interface is not small, but such regions comprise only a small fraction of the domain and have little effect on the dynamics of the rest of the layer. The only assumption is that a sheet does not exert any net horizontal force on the surrounding layer. This assumption may break down if the length of a plume becomes so much greater than the initial wavelength that the flow it drives in the lower fluid becomes dynamically significant.

6. Conclusions

The central concern of this work is the nonlinear interactions between buoyant forces and normal viscous stresses that occur in a buoyantly unstable viscous layer under a shear-free horizontal boundary and over a much less viscous fluid. After the initially uniform thickness of the layer has been perturbed slightly, the early growth of the perturbation is exponential; the perturbation keeps its shape while it grows. But when the nonlinear effects of finite amplitude become important, the thicker parts of the layer thicken more rapidly while the thinner parts thin more slowly, giving in general sharp peaks with broad, flat troughs in between, over a timescale of $8\mu/\Delta\rho g d_1$. The accelerating growth of peaks leads to infinite thickness at some time t_*, and the final catastrophic growth of the peak thickness δ is algebraic: $\delta \approx 8\mu/\Delta\rho g(t_* - t)$ for the two-dimensional case. The axisymmetric case shows essentially the same behaviour. Similar catastrophic growth is also predicted for a power-law fluid, though the power

of $(t_* - t)$ and the coefficient are different. This shows how large-amplitude growth is fundamentally different from small-amplitude growth; large-amplitude effects dramatically enhance the growth of peaks.

The small-slope equations continue to apply to the layer even after the formation of downwelling sheets, except in an asymptotically narrow neighbourhood around each sheet. This is possible because the sheets do not change the horizontal force balance (unless the flow they drive in the lower fluid becomes dynamically significant). Applying the equations up to the singular time shows that at first the sheet should have the local shape $\delta \propto |x|^{-\frac{2}{3}}$, but that afterwards, as the sheet drains the layer, the sheet changes shape to $\delta \propto |x|^{-\frac{1}{2}}$. This behaviour is clarified by a family of similarity solutions, appropriate where δ is large.

This analysis depends on two key assumptions: small interfacial slope and negligible shear stress from fluid 2. When peaks become large enough, the slope becomes large, and the approximate equations become invalid. However, as long as the external shear is negligible, the growth of the disturbance at large slopes is essentially the same as that predicted here (Canright 1987, or Wilson 1988), with catastrophic inverse-time peak growth; while the details of the peak shape are different, this only modifies the prediction of t_* by an $O(1)$ numerical factor. Even so, when the descending sheet becomes long enough, the flow driven in fluid 2 will result in significant shear stress on the interface, retarding the growth and invalidating the approximate equations. (It is also possible, depending on the parameters, that inertia could become important for rapidly growing peaks, or that surface tension could become significant at the highly curves peaks.) So this analysis is not appropriate to describe what happens at the tip of a long descending sheet; e.g. the tip might widen to a bulb, as seen in the experimental plumes of Whitehead & Luther (1975) and the numerical sheets of Newhouse & Pozrikidis (1990) (though both of those works have a no-slip surface, a significant difference). Rather, the present analysis describes the transition from exponential to catastrophic growth of peaks due to finite amplitude, and the subsequent adjustment of the rest of the layer.

The question of whether plumes or sheets are more likely to develop is beyond the scope of this work. Indeed, the dynamic balance considered is independent of wavelength, and so presumably independent of planform as well, at least for Newtonian fluids. However, we speculate that the lack of downwelling plumes in the mantle is due to rheological effects. Assuming that the lithosphere weakens with deformation, the two-dimensional motion leading to sheets allows the deformation to be concentrated at the growing peak while the layer on both sides moves rigidly inward; the axisymmetric flow needed for plumes necessitates significant deformation throughout the entire layer.

To apply these results to the oceanic lithosphere, an order-of-magnitude estimate of the timescale for the formation of a new subduction zone (starting from a finite-amplitude disturbance, say due to mantle convection) by this process is about 0.3 Gyr, or one-tenth the age of the Earth. (This assumes $\mu_1 \sim 10^{25}$ P (Walcott 1973), $d_1 \sim 100$ km, and $\Delta\rho \sim 0.1$ g/cm^3 from a temperature difference $\Delta T \sim 1000$ K with a thermal expansion coefficient $\alpha \sim 3 \times 10^{-5}$/K from a base density of $\rho \sim 3.3$ g/cm^3.) This figure is for illustrative purposes only; the uncertainty in the appropriate viscosity is orders of magnitude. However, if the surface viscosity of the early Earth were orders of magnitude smaller than today, as has been suggested in hot-earth models (Davies 1990), then the timescale would be correspondingly reduced; one possible interpretation would be that modern subduction zones may have their origins early in the Earth's history when the surface layer was sufficiently deformable.

Appendix A. Linearized solution

Here we calculate the small-amplitude growth rates for the non-inertial problem with arbitrary wavelength, depths, and viscosities. (This is an extension of the analysis given by Whitehead & Luther 1975, to include the effects of finite depth in fluid 2.) A more convenient reduced pressure $\tilde{p}$ in each fluid is defined in terms of the total pressure P by

$$P_1 = \tilde{p}_1 + \rho_1 gz, \quad P_2 = \tilde{p}_2 + \rho_2 gz + \Delta\rho g d_1 \qquad (A\ 1a, b)$$

(or from the other reduced pressure p by $p_1 = \tilde{p}_1 + \Delta\rho gz$, $p_2 = \tilde{p}_2 + \Delta\rho g d_1$) so in equilibrium $\tilde{p}$ is zero. Assuming that the interface disturbance varies only in the x-direction and has small amplitude and slope, the resulting two-dimensional problem can be linearized by applying the interface conditions at $z = d_1$. Then the interface conditions (2.4b–d) become

$$\left.
\begin{aligned}
[u]|_1^2 = [\mu(u_z + w_x)]|_1^2 &= 0 \\
[-\tilde{p} + 2\mu w_z]|_1^2 &= \Delta\rho g(\delta - d_1) \\
\delta_t &= w
\end{aligned}
\right\} \quad \text{at} \quad z = d_1,
\qquad
\begin{aligned}
&(A\ 2a) \\
&(A\ 2b) \\
&(A\ 2c)
\end{aligned}$$

where again $[\ ]|_1^2$ indicates the jump in value from fluid 1 to fluid 2. This problem is separable and has a simple analytical solution, assuming that the perturbation is sinusoidal.

The solution is given below, where k is the wavenumber, $a(t)$ is the dimensionless amplitude, $Z \equiv z - (d_1 + d_2)$ is the coordinate in fluid 2, $\alpha \equiv \mu_2/\mu_1$ is the viscosity ratio, and in the coefficients A, B, E, F, and their common denominator D, the abbreviations $\tilde{k} \equiv 2kd_1$, $\tilde{K} \equiv 2kd_2$, $c \equiv \cosh(\tilde{k})$, $C \equiv \cosh(\tilde{K})$, $s \equiv \sinh(\tilde{k})$, $S \equiv \sinh(\tilde{K})$ are used:

$$\delta = d_1[1 + a(t)\cos(kx)], \qquad (A\ 3a)$$

$$\Psi_1 = (\Delta\rho g d_1/\mu_1 k^2)\tfrac{1}{2}a(t)\sin(kx)[A\sinh(kz) + Bkz\cosh(kz)], \qquad (A\ 3b)$$

$$\Psi_2 = (\Delta\rho g d_1/\mu_1 k^2)\tfrac{1}{2}a(t)\sin(kx)[E\sinh(kZ) + FkZ\cosh(kZ)], \qquad (A\ 3c)$$

$$\tilde{p}_1 = (\Delta\rho g d_1)\{-a(t)\,B\cos(kx)\cosh(kz)\}, \qquad (A\ 3d)$$

$$\tilde{p}_2 = (\Delta\rho g d_1)\{-a(t)\,\alpha F\cos(kx)\cosh(kZ)\}, \qquad (A\ 3e)$$

$$A \equiv (-1/D)\{[2(S - \tilde{K}) + \alpha\tilde{k}(C - 1)]\sinh(kd_1)$$
$$+ [\tilde{k}(S - \tilde{K}) + \alpha(\tilde{k}\tilde{K} + 2(C - 1))]\cosh(kd_1)\}, \qquad (A\ 3f)$$

$$B \equiv (2/D)\{(S - \tilde{K} + \alpha\tilde{K})\sinh(kd_1) + \alpha(C - 1)\cosh(kd_1)\}, \qquad (A\ 3g)$$

$$E \equiv (1/D)\{[2\alpha(s - \tilde{k}) + \tilde{K}(c - 1)]\sinh(kd_2)$$
$$+ [\alpha\tilde{K}(s - \tilde{k}) + \tilde{K}\tilde{k} + 2(c - 1)]\cosh(kd_2)\}, \qquad (A\ 3h)$$

$$F \equiv (-2/D)\{[\alpha(s - \tilde{k}) + \tilde{k}]\sinh(kd_2) + (c - 1)\cosh(kd_2)\}, \qquad (A\ 3i)$$

$$D \equiv (S - \tilde{K})(s + \tilde{k}) + 2\alpha(Cc - 1 + \tilde{K}\tilde{k}) + \alpha^2(S + \tilde{K})(s - \tilde{k}). \qquad (A\ 3j)$$

Then from $\delta_t = \omega(z = d_1)$ we get the growth rate:

$$a(t) = a(0)\,e^{\sigma t}, \qquad \sigma = (\Delta\rho g d_1/\mu_1)\,\tilde{\sigma}, \qquad (A\ 4a, b)$$

$$\tilde{\sigma} = \frac{1}{\tilde{k}}\,\frac{(S - \tilde{K})(c - 1) + \alpha(s - \tilde{k})(C - 1)}{(S - \tilde{K})(s + \tilde{k}) + 2\alpha(Cc - 1 + \tilde{K}\tilde{k}) + \alpha^2(S + \tilde{K})(s - \tilde{k})}. \qquad (A\ 4c)$$

The symmetry of the problem is apparent in the solution. Thus, without loss of generality, assume that fluid 2 is the deeper layer: $\tilde{K} \geqslant \tilde{k}$.
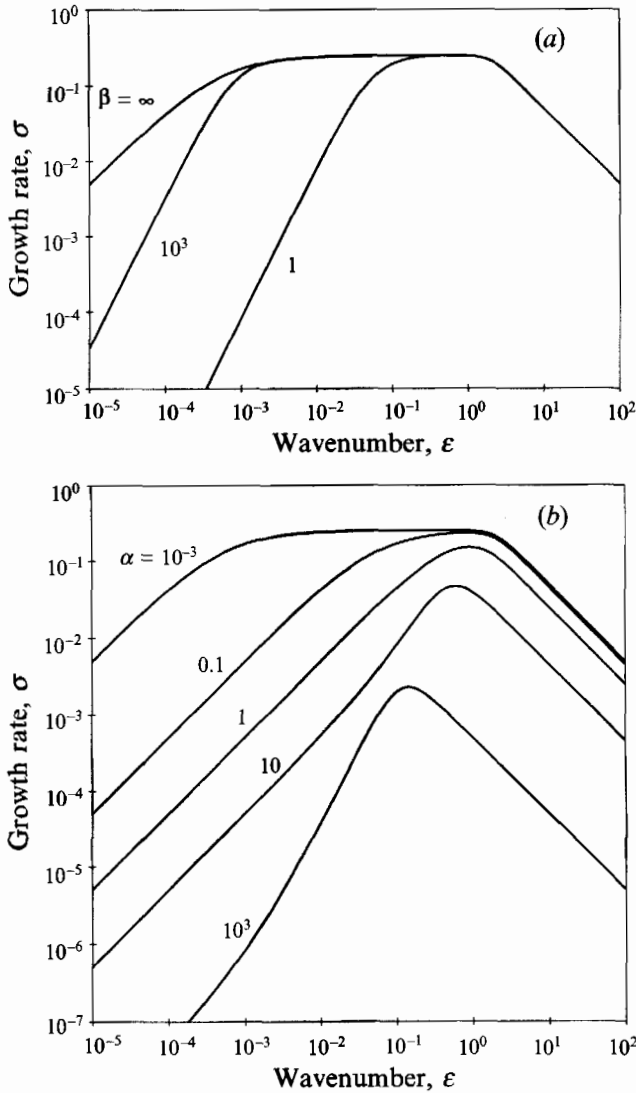
FIGURE 7. Linearized growth rate $\tilde{\sigma}$ (A 4c) as a function of dimensionless wavenumber ϵ: (a) for viscosity ratio $\alpha \equiv \mu_2/\mu_1 = 10^{-3}$ and depth ratios $\beta \equiv d_2/d_1 = 1$, 10^3, and ∞; (b) for deep fluid ($\beta = \infty$) and $\alpha = 10^{-3}$, 0.1, 1, 10, 10^3.

This solution is governed by three dimensionless parameters: the non-dimensional wavenumber $\tilde{k}$ (or ϵ), the depth ratio $\beta \equiv d_2/d_1 = \tilde{K}/\tilde{k}$, and the viscosity ratio $\alpha \equiv \mu_2/\mu_1$. Note that $\tilde{\sigma}$ is a monotonically decreasing function of α: if we increase μ_2 while μ_1 stays constant the growth rate can only decrease. In the limit $\beta \to \infty$ then (A 4c) reduces to

$$\tilde{\sigma} = \frac{1}{\tilde{k}} \frac{(c-1)+r(s-\tilde{k})}{(s+\tilde{k})+2rc+r^2(s-\tilde{k})}, \tag{A 5}$$

which is just the result of Whitehead & Luther (1975). Figure 7(a) shows the effects of finite depth for $\alpha \ll 1$; figure 7(b) shows the effects of viscosity ratio on $\tilde{\sigma}(\tilde{k})$ for $\beta = \infty$.
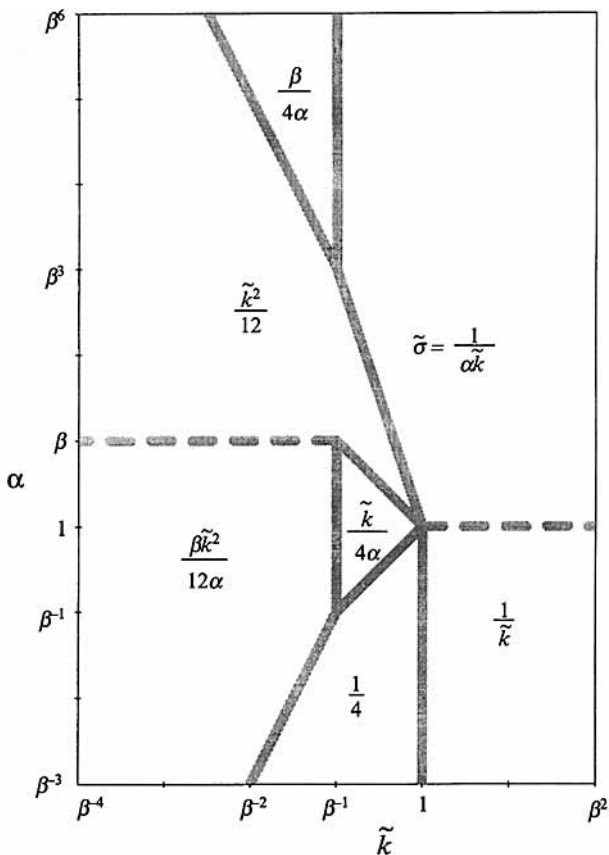
FIGURE 8. Linearized growth regimes for $\beta \gg 1$ in the $(\tilde{k}, \alpha)$ parameter plane, showing the asymptotic growth rates $\tilde{\sigma}$ in each regime. (Dashed lines indicate change of rate-controlling viscosity.)

When $\beta \gg 1$ there are well-defined regimes of growth where different force balances are dominant. These are shown schematically, with the corresponding growth rates, in figure 8. In discussing the various growth mechanisms below, it should be kept in mind that the same mechanisms continue to apply as long as the slope of the interface remains small, which for long waves includes large-amplitude growth.

For sufficiently short waves ($\tilde{k} \gg \min(1, \max(\beta^{-1}, \alpha^{-\frac{1}{3}}))$) the disturbance sees neither boundary and $\tilde{\sigma} \to [\tilde{k}(1+\alpha)]^{-1}$, so if one viscosity is much larger, that one limits the growth. The dominant mechanism here is that the vertical motion of the interface is resisted by normal viscous stresses in the more viscous fluid, and the growth rate diminishes with decreasing wavelength.

At the other extreme, for sufficiently long waves ($\tilde{k} \ll \min(\beta^{-1}, (\beta/\alpha)^{\frac{1}{2}}, (\alpha\beta)^{\frac{1}{3}})$) the boundaries confine the flow to be mainly horizontal, limited by shear stresses at the interface. Then $\tilde{\sigma} \to \tilde{k}^2(1+\beta/\alpha)/12$, and the controlling viscosity depends on whether $\alpha > \beta$.

Between these extremes, the waves are long compared to layer 1 so the motion of the interface is primarily horizontal, and there are four different regimes. In one ($\alpha^{-1} \ll \tilde{k} \ll \alpha^{-\frac{1}{3}}$, $1 \ll \alpha \ll \beta^3$), fluid 2 is relatively immobile and the growth is limited by the shear across layer 1, giving the same growth rate as the previous case, i.e. $\tilde{k}^2/12$. (This possibility was apparently overlooked by Whitehead & Luther.) In another ($\beta^{-1} \ll \tilde{k} \ll$

min (α, α^{-1})), the slight resistance of fluid 2 (the rate-controlling viscosity is μ_2) gives a small shear gradient across layer 1, which over the long wavelength is sufficient to balance the buoyancy, giving $\tilde{\sigma} \to \tilde{k}/4\alpha$.

In the other two regimes, the less viscous fluid is effectively passive, and the primarily horizontal motion of the more viscous layer is limited by normal viscous stresses. The resulting growth rate is nearly independent of wavelength, and includes the maximum growth rate possible for a given viscosity contrast α where this behaviour occurs. (For other α, i.e. $1 \ll \alpha \ll \beta^3$, we expect the fastest growth at the crossover between short- and long-wave behaviour.) When fluid 2 is much more viscous ($\alpha \gg \beta^3$), this regime $((\beta/\alpha)^{\frac{1}{2}} \ll \tilde{k} \ll \beta^{-1})$ gives $\tilde{\sigma} \to \beta/4\alpha$, while for fluid 1 more viscous ($\alpha \ll 1$) this regime $(\max(\alpha, (\alpha\beta)^{\frac{1}{2}}) \ll \tilde{k} \ll 1)$ gives $\tilde{\sigma} \to \frac{1}{4}$.

In the last case, examining the broad peak more closely shows that, for $\beta^{-5} \ll \alpha \ll 1$, $\tilde{\sigma} \approx \frac{1}{4}(1-(\alpha/\tilde{k}+\tilde{k}^4/720))$. This broad maximum peaks at $\tilde{k}_{max} \approx (180\alpha)^{\frac{1}{5}} = 2.8\alpha^{\frac{1}{5}}$ and $\tilde{\sigma}_{max} \approx \frac{1}{4}(1-0.44\alpha^{\frac{4}{5}})$. As an indication of the flatness of this peak, for the range $\alpha^{\frac{4}{5}} < k < 5.2\alpha^{\frac{1}{20}}$, $\tilde{\sigma} \geqslant \frac{1}{4}(1-\alpha^{\frac{1}{5}})$. When $\alpha \ll \beta^{-5}$, the finite depth modifies the maximum growth rate, giving $\tilde{\sigma} \approx \frac{1}{4}(1-(3\alpha/\beta\tilde{k}^2+\tilde{k}^4/720))$ with a broad peak at $\tilde{k}_{max} \approx 3.2(\alpha/\beta)^{\frac{1}{6}}$ and $\tilde{\sigma}_{max} \approx \frac{1}{4}(1-0.44(\alpha/\beta)^{\frac{2}{3}})$.

The present work is only concerned with the case of a thin, viscous layer over a less viscous, deep layer, so $\alpha \ll 1$ and $\beta \gg 1$. We further restrict our consideration to the mechanism giving the fastest growth, i.e. the last regime considered above, where $\tilde{\sigma} \approx \frac{1}{4}$. The lowest-order finite-amplitude analysis (§3) therefore predicts that the growth is independent of wavelength.

Appendix B. Power-law fluid

The long-wave analysis of §3 is not limited to Newtonian fluids. The important point is that both surfaces of the layer are shear-free, so throughout the layer shear stresses are $O(\epsilon)$ smaller than normal stresses, and the latter are independent of z to $O(\epsilon^2)$. (This assumes that the lower fluid is passive and effectively hydrostatic; the restriction this applies to wavelength will depend on the rheology and depth of fluid 2.) Hence the horizontal force balance (3.5), (3.6) applies for any rheology.

Here we consider a layer of fluid with a power-law rheology, subject to a disturbance independent of y. Then the constitutive relation can be written in the form

$$\tau_{xx} = -\tau_{zz} = 2\mu_r \operatorname{sgn}(u_x)|u_x|^{1/m}, \qquad \text{(B 1)}$$

where μ_r has appropriate units and $m > 1$ for a fluid that weakens with increasing strain rate. Eliminating τ_{xx} and u as before yields a single Lagrangian equation describing the evolution of the thickness of the layer as we follow a material cross-section, in dimensionless form:

$$\frac{D\delta}{Dt} = \operatorname{sgn}(\delta-d_e(t))\,\delta\left[\frac{|\delta^2-d_e^2(t)|}{\delta}\right]^m, \qquad \text{(B 2)}$$

using the same scales as before, except for the new timescale $(8\mu_r/\Delta\rho gd_1)^m$. For the special case of a Newtonian fluid ($m = 1$) this reduces to (3.13). To simplify the notation, we will assume that m is an odd integer.

For an infinitely long layer with a localized disturbance (i.e. constant end forces: $d_e = 1$)

$$\frac{D\delta}{Dt} = \frac{(\delta^2-1)^m}{\delta^{m-1}}. \qquad \text{(B 3)}$$
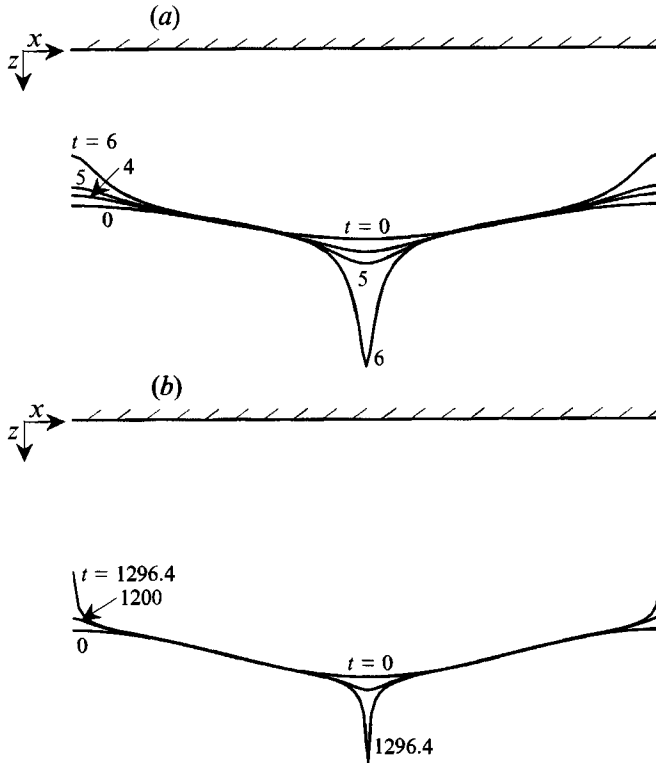
FIGURE 9. Interface profiles $\delta(x)$ for a power-law fluid, for an initial sinusoidal perturbation of amplitude 0.1, for the constant-wavelength conditions $(L = 1)$: (a) power-law exponent $m = 3$, at times $t = 0, 4, 5$, and 6 $(t_* \approx 6.08)$; (b) $m = 7$ and $t = 0, 1200.0$, and 1296.4 $(t_* \approx 1296.5)$. For higher m the deforming region is more compact, and the profile tends toward straight lines between the deforming regions.

This can be integrated by parts. For example, if $m = 3$

$$\tau(\delta) = \frac{\delta}{4(\delta^2-1)^2} + \frac{\delta}{8(\delta^2-1)} + \frac{1}{16}\ln\left|\frac{\delta-1}{\delta+1}\right|, \tag{B 4}$$

where $\tau(\delta) \equiv t_* - t$ is the time remaining before the thickness of the fluid cross-section goes to ∞ or 0.

While the amplitude $a \equiv \delta - 1$ remains small, the approximate solution is

$$a \approx \frac{a_0}{[1-(m-1)\,2^m\,a_0^{m-1}t]^{1/(m-1)}}, \tag{B 5}$$

where a_0 is the initial amplitude. (This algebraic growth is quite different from the small-amplitude exponential growth for Newtonian rheology.) This slow growth lasts for a period of roughly $\Delta t \sim 1/[(m-1)2^m a_0^{m-1}]$. For large amplitudes, the growth again becomes algebraic in the time remaining before the singularity is reached at $t = t_*$:

$$\delta \approx 1/[m(t_*-t)]^{1/m}, \quad \delta_0 > 1 \tag{B 6a}$$

$$\delta \approx [m(t_*-t)]^{1/m}, \quad \delta_0 < 1. \tag{B 6b}$$

This catastrophic growth occurs over a timescale $\Delta t \sim 1/m$ (or in dimensional terms $(8\mu_r/\Delta\rho gh)^m/m$).
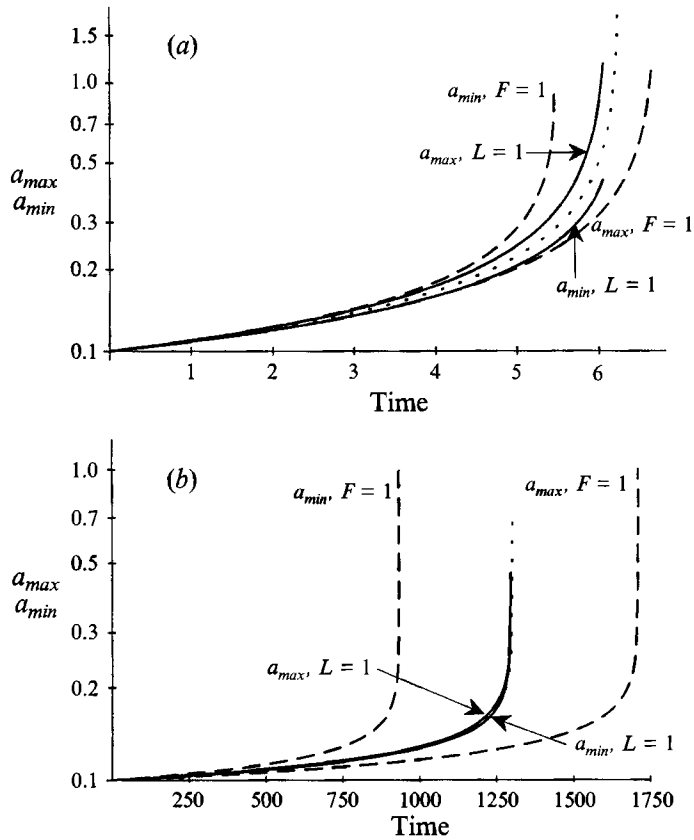
FIGURE 10. Growth of the disturbance amplitude over time for a power-law fluid given an initial perturbation amplitude of 0.1: constant-wavelength $L = 1$ (solid), constant end-force $F = 1$ (dashed), and small-amplitude approximation (B 5) (dotted). (*a*) $m = 3$; (*b*) $m = 7$. For constant force, the trough (a_{min}) would pinch off long before the peak (a_{max}) became infinite, but the constant-wavelength condition makes the peaks less stable and troughs more stable. For higher m, the growth abruptly becomes rapid.

As in the Newtonian case, a disturbed region under constant end forces will tend to stretch out in the x-direction. To keep the wavelength constant, the end forces must vary in time to give

$$\int_0^L \left[\frac{\delta^2 - d_e^2(t)}{\delta} \right]^m \mathrm{d}x = 0. \tag{B 7}$$

Layer profiles calculated using this condition are shown in figure 9 for $m = 3$ and $m = 7$, from an initial sinusoidal disturbance. Profiles for the constant-end-force condition (not shown) are qualitatively similar. The effect of increasing m is seen to be concentration of the deformation into narrow regions at the centres of peaks and troughs, while elsewhere the profile becomes linear in x.

Figure 10 shows how the initial slow growth suddenly becomes catastrophic after a certain threshold has been reached (more so for higher m). For the constant-force condition, a trough reaches this threshold and necks off much sooner than a peak of equal initial amplitude blows up. The constant-wavelength condition, however, causes peaks to grow sooner than troughs.

Regardless of the end conditions, when peaks get large (compared to the current

equilibrium thickness), the large-amplitude effects still produce catastrophic growth algebraic in the time remaining ($\delta \propto 1/(t_* - t)^{1/m}$), giving infinite thickness in finite time, as for a Newtonian fluid.

Appendix C. Large-amplitude similarity solution

The equations appropriate to large-amplitude disturbances (for the two-dimensional case) admit a rich family of similarity solutions, which illustrate a variety of behaviour. While such solutions demand particular initial conditions, nonetheless they can be interpreted as good local approximations for situations arising from arbitrary initial conditions. Two cases are of particular relevance to sheet formation: one describes how a smooth finite peak evolves to an infinite singularity, the other describes how that first singularity changes shape as the sheet evolves.

For large amplitudes d_e is negligible, and the Eulerian equations are

$$\delta_t + (u\delta)_x = 0, \qquad \delta + u_x = 0. \tag{C 1 a, b}$$

We assume a similarity solution of the following form:

$$x = a(\tau)\,\xi, \quad \delta = A(\tau)\,f(\xi), \quad u = a(\tau)\,A(\tau)\,g(\xi), \tag{C 2}$$

where $\tau \equiv t - t_*$ is the time relative to the singular time t_*. Substitution shows that similarity requires both A'/A^2 and $a'/(aA)$ to be constants.

Choosing the scale of A (provided $A' \neq 0$) gives

$$A(\tau) = 1/\tau. \tag{C 3a}$$

Of course, δ must be non-negative, so solutions with $f \geqslant 0$ will apply only for $\tau \geqslant 0$, when A is decreasing, and those with $f \leqslant 0$ will apply for $\tau \leqslant 0$, when $-A$ is increasing catastrophically to $\tau = 0$. The second constant, say λ, implies

$$a(\tau) = |\tau|^\lambda. \tag{C 3b}$$

For $\tau > 0$, positive λ gives a profile that spreads out in the x-direction, while for negative λ the profile contracts; the converse is true for $\tau < 0$.

The system (C 1) becomes

$$-f - \lambda\xi f' + (fg)' = 0, \quad f + g' = 0. \tag{C 4a, b}$$

The solution involves two arbitrary constants C and D and a change of variables (as long as $\lambda \neq 0, 1$), corresponding to a different inertial reference frame:

$$\zeta \equiv \xi - C/(\lambda^2 - \lambda), \quad q(\zeta) \equiv g(\xi) - C/(\lambda - 1). \tag{C 5}$$

The solution is given implicitly by

$$\zeta = q + \operatorname{sgn}(\zeta - q)\,D|q|^k, \quad f = -1/[1 + \operatorname{sgn}(q(\zeta - q))\,kD|q|^{k-1}], \tag{C 6a, b}$$

where $k \equiv \lambda/(\lambda - 1)$ and $D > 0$. This is the general solution; a phase-plane analysis verifies that this gives all solutions (for $A(t)$ not constant, $\lambda \neq 0, 1$) except the trivial solutions $f = 0$ and $f = -1$. This solution describes a variety of behaviour, depending primarily on λ and on which branch of the solution is chosen. The constants C and D affect the x origin and scale, respectively.

For example, consider $\lambda > 1$ (so $k > 1$), $C = 0$, $D = 1$, and the branch where $\operatorname{sgn}(\xi - g) = \operatorname{sgn}(\xi) = \operatorname{sgn}(g)$:

$$\xi = g + \operatorname{sgn}(g)\,|g|^k, \quad f = -1/[1 + k|g|^{k-1}]. \tag{C 7a, b}$$

Since $f \leqslant 0$, this solution only applies for $\tau \leqslant 0$; it describes the growth of a finite peak up to the singular time when δ becomes infinite. The asymptotics in ξ reveal the behaviour

$$\delta \to [1 - k|\tau|^{-k}|x|^{k-1}]/|\tau|, \quad u \to -x/|\tau| \quad \text{as} \quad |\xi| \to 0; \tag{C 7c}$$

$$\delta \to |x|^{-1/\lambda}/k, \quad u \to -\operatorname{sgn}(x)|x|^{1/k} \quad \text{as} \quad |\xi| \to \infty. \tag{C 7d}$$

The first (C 7c) applies for x near the origin ($|x| \ll |\tau|^\lambda$). The peak is of fairly general shape, but to be analytic in x, k must be an odd integer. The second (C 7d) applies far from the origin early on ($\tau \ll 0$), but applies ever nearer until at the singular time, it applies for all x. The asymptotic shape (C 7d) is independent of time; as the peak grows it fills in the profile of the integrable negative power of x. For a smooth peak, $k = 3$, $\lambda = \frac{3}{2}$ and at the singular time $\delta \propto |x|^{-\frac{2}{3}}$ (for any D).

As a second example, $\lambda > 1$, $C = \operatorname{sgn}(\xi)$, $D = (\lambda-1)^k/\lambda$, and the branch where $\operatorname{sgn}(\xi) = -\operatorname{sgn}(g)$:

$$\xi = g - \operatorname{sgn}(g)\lambda^{-1}[((\lambda-1)|g|+1)^k - 1], \tag{C 8a}$$

$$f = 1/[((\lambda-1)|g|+1)^{k-1} - 1], \tag{C 8b}$$

which describes a sheet, symmetric in x, for $\tau \geqslant 0$. Asymptotically

$$\delta \to 1/[\tau^{1-\lambda/2}(2|x|)^{\frac{1}{2}}], \quad u \to -\operatorname{sgn}(x)(2|x|)^{\frac{1}{2}}/\tau^{1-\lambda/2} \quad \text{as} \quad |\xi| \to 0; \tag{C 8c}$$

$$\delta \to (\lambda|x|)^{-1/\lambda}, \quad u \to -\operatorname{sgn}(x)(\lambda|x|)^{1/k}/(\lambda-1) \quad \text{as} \quad |\xi| \to \infty. \tag{C 8d}$$

At the singular time ($\tau = 0$), the time-independent profile (C 8d) applies everywhere; this example shows what happens to an initial profile proportional to an integrable negative power of x. (By a different choice of C and D, the profile (C 8d) could be made to match (C 7d) exactly.) For $\tau > 0$, (C 8c) applies near the origin; regardless of the starting x-dependence, the shape around the singularity (sheet) becomes proportional to $1/|x|^{\frac{1}{2}}$. If $\lambda < 2$ then the square-root singularity and the corresponding strength of the sink at the origin decay with time, as the layer drains away. (This would be true for an initially smooth profile like (C 7c) with $\lambda = \frac{3}{2}$.) Conversely, for $\lambda > 2$, the singularity grows, as fluid comes in from the sides faster than it can be disposed of. The special case $\lambda = 2$ gives a steady sheet. There are also related solutions for $\lambda = 0$, $0 < \lambda < 1$, and $\lambda = 1$, which have the same asymptotic shapes (C 8c, d), except that, for $|\xi| \to \infty$, the forms for u are different, and for $\lambda = 0$, $\delta \to e^{-|x|}/t$ as $|\xi| \to \infty$.

Briefly, the other types of behaviour governed by the similarity solution are as follows. For $\tau \leqslant 0$, i.e. profiles growing to the singular time, there are four: (i) a zero minimum of shape $|x|^k$, $k > 0$, locally time-independent, that far away levels off to approach $1/|\tau|$; (ii) a profile that approaches zero as $x \to -\infty$ and $1/|\tau|$ as $x \to +\infty$; (iii) a symmetric finite minimum flanked by sheets (which could be extended periodically); and (iv) a sheet whose sides levels off to approach $1/|\tau|$, rather than zero. For $\tau \geqslant 0$, where the profile starts at the singular time and diminishes thereafter, there is only one other case: a zero minimum flanked by sheets (which could extend periodically). The steady-shape case of $A(\tau) = 1$, so $a(\tau) = e^{\lambda\tau}$, gives either an isolated sheet, or a zero minimum where $|\delta_x| \to \infty$ surrounded by sheets (possibly periodic). Note that solutions with the same $A(\tau)$ and λ but different C and D can be 'cut and pasted' together to give other similarity profiles; if g and g' are continuous this will produce reasonable results. All cases with sheets show the same $1/|x|^{\frac{1}{2}}$ shape.

REFERENCES

AMARANATH, T. & RAJAPPA, N. R. 1976 A study of Taylor instability of superposed fluids. *Acta Mech.* **24**, 87–97.

AREF, H. & TRYGGVASON, G. 1989 Model of Rayleigh–Taylor instability. *Phys. Rev. Lett.* **62**, 749–752.

BAKER, G. R. & MEIRON, D. I. 1984 Boundary integral methods for axisymmetric and three-dimensional Rayleigh–Taylor instability problems. *Physica* **12D**, 19–31.

BAKER, L. & FREEMAN, J. R. 1981 Heuristic model of the nonlinear Rayleigh–Taylor instability. *J. Appl. Phys.* **52**, 655–663.

BELLMAN, R. & PENNINGTON, R. H. 1954 Effects of surface tension and viscosity on Taylor instability. *Q. Appl. Maths* **12**, 151–162.

CANRIGHT, D. R. 1987 A finite-amplitude analysis of the buoyant instability of a highly viscous film over a less viscous half-space. PhD thesis, University of California, Berkeley.

CANRIGHT, D. R. & MORRIS, S. 1993 Long-wave buoyant instability of a thermo-viscous layer beneath a suddenly cooled plane. (In preparation.)

CHANDRASEKHAR, S. 1961 *Hydrodynamic and Hydromagnetic Instability.* Oxford University Press.

DAVIES, G. F. 1990 Heat and mass transport in the early earth. In *Origin of the Earth* (ed. H. E. Newsom & J. H. Jones), pp. 175–194. Oxford University Press.

DIENES, J. K. 1978 Method of generalized coordinates and an application to Rayleigh–Taylor instability. *Phys. Fluids* **21**, 736–744.

DRAZIN, P. G. 1969 Non-linear internal gravity waves in a slightly stratified atmosphere. *J. Fluid Mech.* **36**, 433–446.

DUSSAN V., E. B. 1975 Hydrodynamic stability and instability of fluid systems with interfaces. *Arch. Rat. Mech. Anal.* **57**, 363–379.

EMMONS, H. W., CHANG, C. T. & WATSON, B. C. 1960 Taylor instability of finite surface waves. *J. Fluid Mech.* **7**, 177–193.

HARLOW, F. H. & WELCH, J. E. 1966 Numerical study of large-amplitude free-surface motions. *Phys. Fluids* **9**, 842–851.

KULL, H. J. 1986 Nonlinear free-surface Rayleigh–Taylor instability. *Phys. Rev.* A **33**, 1957–1967.

KULL, H. J. 1991 Theory of the Rayleigh–Taylor instability. *Phys. Rep.* **206**, 197–325.

LEWIS, D. J. 1950 The instability of liquid surfaces when accelerated in a direction perpendicular to their planes, II. *Proc. R. Soc. Lond.* A **202**, 81–96.

MENIKOFF, R., MJOLSNESS, R. C., SHARP, D. H. & ZEMACH, C. 1978 Initial value problem for Rayleigh–Taylor instability of viscous fluids. *Phys. Fluids* **21**, 1674–1687.

NAYFEH, A. H. 1969 On the non-linear Lamb–Taylor instability. *J. Fluid Mech.* **38**, 619–631.

NEWHOUSE, L. A. & POZRIKIDIS, C. 1990 The Rayleigh–Taylor instability of a viscous liquid layer resting on a plane wall. *J. Fluid Mech.* **217**, 615–638.

OTT, E. 1972 Nonlinear evolution of the Rayleigh–Taylor instability of a thin layer. *Phys. Rev. Lett.* **29**, 1429–1432.

RAYLEIGH, LORD 1883 Investigation of the character of an incompressible heavy fluid of variable density. *Proc. Lond. Math. Soc.* **14**, 170–197.

SHARP, D. H. 1984 An overview of Rayleigh–Taylor instability. *Physica* **12 D**, 3–18.

TAYLOR, G. I. 1950 The instability of liquid surfaces when accelerated in a direction perpendicular to their planes. I. *Proc. R. Soc. Lond.* A **201**, 192–196.

TRYGGVASON, G. 1988 Numerical simulations of the Rayleigh–Taylor instability. *J. Comput. Phys.* **75**, 253–282.

WALCOTT, R. I. 1973 Structure of the earth from glacio-isostatic rebound. *Ann. Rev. Earth Planet. Sci.* **1**, 15–37.

WHITEHEAD, J. A. & LUTHER, D. S. 1975 Dynamics of laboratory diapir and plume models. *J. Geophys. Res.* **80**, 705–717.

WILSON, S. D. R. 1988 The slow dripping of a viscous fluid. *J. Fluid Mech.* **190**, 561–570.